DOI: 10.1002/ejic.201000325

Syntheses at Elevated Temperature and Structures of Lanthanoid/Alkaline Earth Heterobimetallic Derivatives of 2-Methyl-8-hydroxyquinoline

Glen B. Deacon,[a] Craig M. Forsyth,[a] Peter C. Junk,*[a] and Aron Urbatsch[a]

Keywords: Lanthanides / Alkaline earth metals / Structure elucidation / N, O ligands

Rearrangement reactions between $Ln(MQ)_3$ and $AE(MQ)_2$ (MQ = 8-quinaldinolate) at 200–300 °C in a 1,2,4,5-tetramethylbenzene (TMB) flux afforded the homoleptic heterobimetallic complexes $[Ln_2AE(MQ)_8]$ (Ln = Eu, Gd, Tb, Er with AE = Mg; Ln = La, Eu with AE = Ca) and $[Eu_3Ba(MQ)_{11}]\cdot 2TMB$. From an attempt to prepare $[La_2Mg(MQ)_8]$, $[Mg_4(MQ)_8]$ was isolated, and it was also obtained with the heterobimetallics from syntheses in which Ln = Eu, Gd, Tb. Surprisingly, $[Er_3(MQ)_7CO_3]$ was isolated from an attempted synthesis of $[Er_2Ca(MQ)_8]$, and the Eu analogue was prepared from $Eu(MQ)_3$ and $CaCO_3$ in TMB at 210 °C. The $[Ln_2AE(MQ)_8]$ complexes have a trinuclear structure with a linear or nearly linear Ln–AE–Ln array. Octacoordinate Ln atoms have one terminal chelating (N, O) MQ ligand and three chelating-bridging MQ ligands that link to AE through the phenolic oxygen atoms, leading to hexacoordination of AE. In $[Eu_3Ba(MQ)_{11}]\cdot 2TMB$, an Eu atom is positioned above the Ba–Eu vector of a somewhat bent Eu–Ba–Eu unit. All atoms are octacoordinate, and the structure features μ_3-η^2(N,O):η^1(O):η^1(O) MQ ligands in addition to terminal chelating and chelating-bridging μ-η^2(N,O):η^1(O) MQ groups observed in $[Ln_2AE(MQ)_8]$ complexes. The three modes of ligation are also observed in $[Mg_4(MQ)_8]$ where Mg is hexacoordinate but with two different arrays. $[Ln_3(MQ)_7CO_3]$ complexes have a perpendicular Ln–Ln–Ln arrangement with two octacoordinate metal atoms flanking a heptacoordinate one. Carbonate binding features the new η^1(O)-μ_3-η^1(O′):η^1(O′):η^1(O′)-η^1(O″) ligation mode. The carbonate ligand chelates to each of the outer Ln atoms, which are also linked to one chelating and two chelating-bridging MQ ligands. Attached to the central Ln atom is a carbonate oxygen atom, four oxygen atoms from chelating-bridging MQ ligands and a terminal MQ chelate.

Introduction

Lanthanoid 8-quinolinolates $[Ln(OQ)_3]$ first attracted attention as gravimetric reagents owing to their insolubility.[1] Recently, functionalised and elaborated 8-hydroxyquinoline ligands have been prominent in the development of luminescent and light-emitting materials based on lanthanoid ions, both in heterobimetallic[2–4] and homometallic[5–8] lanthanoid complexes. Derivatisation of 8-hydroxyquinoline has added further donor atom capacity and enhanced solubility, thereby facilitating syntheses.[3] However, insolubility of the parent lanthanoid 8-quinolinolates makes crystal formation difficult, and structures of only two complexes of this type $[Ln_3(OQ)_9]\cdot$solv (Ln = Er, solv = MeCN; Ln = Ho, solv = HOQ) have been reported[9,10] {see also the extremely novel $[Sc(\eta^2\text{-}MQ)_2(\eta^1\text{-}MQ)(\eta^1\text{-}HMQ)]\cdot 2H_2O$[11] and the anionic homoleptic $NH_4[Er(OQ')_4]$ (OQ′ = 5,7-dibromo-8-quinolinol[7])}. Both are trinuclear, well-encapsulated species of extremely low solubility. Solubility problems also make it a challenge to prepare homoleptic f-element/d- or alkaline earth element heterobimetallics of the parent HOQ and to obtain crystalline products for X-ray crystallography. We have presented preliminary accounts of three pseudo-solid-state synthetic approaches to crystalline Ln/M heterobimetallic 8-quinolinolates, namely by: (i) reaction of a mixture of calcium and neodymium metals with 8-hydroxyquinoline at elevated temperatures to afford $[Nd_2Ca(OQ)_8]$ as single crystals in low yield together with bulk red amorphous glass,[12] (ii) reaction of HOQ with a $LaNi_5$ alloy at elevated temperatures giving $[LaNi_2(OQ)_7]$[13] and (iii) rearrangement of a mixture of $Ln(OQ)_3$ and either $Ca(OQ)_2$ or $Co(OQ)_2$ in a 1,2,4,5-tetramethylbenzene flux at 200–300 °C to yield $[Eu_2Ca(OQ)_8]$ or $[LaCo_2(OQ)_7]$, respectively.[14] 8-Hydroxyquinaldine (HMQ) is also a gravimetric reagent with a similar solubility profile for metal complexes, thereby posing similar problems for the synthesis of f-element/d- or alkaline earth element heterobimetallics. The close proximity of the methyl group to the N-donor centre may impose steric constraints on heterobimetallic complex formation. We now report a study of the formation of lanthanoid/alkaline earth (AE) heterobimetallics $[Ln_2AE(MQ)_8]$ (AE = Mg or Ca) and $[Eu_3Ba(MQ)_{11}]\cdot 2TMB$ by rearrangement reactions of the appropriate $Ln(MQ)_3$ and $AE(MQ)_2$ complexes at elevated temperatures together with a discussion of their structures. Synthetic complications have led to an elevated-temperature preparation of $[Ln_3(MQ)_7CO_3]$ (Ln = Eu, Er) complexes with a new mode

[a] School of Chemistry, Monash University, Clayton, Vic. 3800, Australia
E-mail: peter.junk@sci.monash.edu.au

Supporting information for this article is available on the WWW under http://dx.doi.org/10.1002/ejic.201000325.

of carbonate coordination. The method has implications for syntheses of a wider field of 8-hydroxyquinoline mixed-ligand complexes. Two mixed-ligand OQ/or substituted OQ acetate complexes are known, viz. $[Ln_3(OQ)_8(O_2CCH_3)]$ (Ln = Er,[7] Yb[15]), but with stoichiometry and structure different from the present carbonato species.

Results and Discussion

Synthesis and Characterisation

A range of $Ln(MQ)_3$ and $AE(MQ)_2$ derivatives were prepared by standard precipitation methods in water, and they were thoroughly dried before use in syntheses. All heterobimetallic compounds were prepared by rearrangement reactions between appropriate $Ln(MQ)_3$ and $AE(MQ)_2$ derivatives in a 1,2,4,5-tetramethylbenzene (TMB) flux at 200–300 °C, but different outcomes were observed for different combinations of reactants [Reaction (1)].

$$2nLn(MQ)_3 + nAE(MQ)_2 \xrightarrow{TMB} n[Ln_2AE(MQ)_8]\cdot xTMB \quad (1)$$

Complexes n[Ln$_2$Mg(MQ)$_8$]·xTMB (Ln = Eu, Gd, Tb; n = 3, x = 1; Ln = Er; n = 1, x = 0)

After preparations by Reaction (1) at 210 °C, single crystals of $n[Ln_2Mg(MQ)_8]\cdot xTMB$ (Ln = Eu, Gd, Tb; n = 3, x = 1) were isolated by handpicking. In addition, single crystals of $[Mg_4(MQ)_8]$ were separated for Ln = Gd. Both compounds were detected in the bulk powder. Preparation of complexes Ln = Eu, Er at 270 °C gave solely crystals of the heterobimetallic compound. These latter results suggest that higher temperatures favour formation of heterobimetallics. In addition, the amounts of $[Mg_4(MQ)_8]$ produced decreased with the decrease in ionic radii, until with Ln = Er, only single crystals of $[Er_2Mg(MQ)_8]$ were obtained, and only this compound was detected in the bulk powder. Moreover, attempted preparation of $[La_2Mg(MQ)_8]$ by Reaction (1) led to the formation of single crystals of $[Mg_4(MQ)_8]$ and bulk powder, in which monometallic $[Mg_4(MQ)_8]$ was detected by X-ray powder diffraction. As no other product could be detected, the residual $La(MQ)_3$ must be amorphous. It is also noteworthy that $[Er_2Mg(MQ)_8]$ was obtained unsolvated in contrast to Ln = Eu, Gd, Tb. For comparison, $[Eu_2Mg(OQ)_8]$ was prepared in an analogous manner at 210 °C and was obtained unsolvated by TMB, in contrast to the related MQ synthesis.

Complexes [Ln$_2$Ca(MQ)$_8$] (Ln = La, Eu)

Both complexes were obtained unsolvated by TMB by Reaction (1) and were isolated in low yield as single crystals, whilst the powder contained the heterobimetallics and some unidentified impurities. From an analogous attempt to prepare $[Eu_2Ba(MQ)_8]$ by Reaction (1), a few single crystals of $[Eu_3Ba(MQ)_{11}]\cdot 2TMB$ were isolated, which is a departure from the usual trimetallic stoichiometry [Reaction (2)].

$$3Eu(MQ)_3 + Ba(MQ)_2 \xrightarrow{TMB} [Eu_3Ba(MQ)_{11}]\cdot 2TMB \quad (2)$$

Complexes [Ln$_3$(MQ)$_7$CO$_3$] (Ln = Eu, Er)

From an attempt to prepare $[Er_2Ca(MQ)_8]$ by Reaction (1), a modest yield of single crystals of $[Er_3(MQ)_7CO_3]$ was separated by handpicking. Powder diffraction of the bulk product showed solely lines of the same compound, but an amorphous Ca complex must also be present. A more deliberate synthesis of $[Eu_3(MQ)_7CO_3]$ was attempted from $Eu(MQ)_3$ and $CaCO_3$ in a TMB flux, and a low yield of single crystals of the target compound was obtained [Reaction (3)]. The formation of the Er derivative can be attributed to the usage of an aged sample of the alkaline earth MQ chelate. It is presumed that this sample absorbed atmospheric CO_2 over time, forming some $CaCO_3$. The successful synthesis of the Eu analogue with the addition of $CaCO_3$ [utilised instead of $Ca(MQ)_2$] is consistent with this explanation.

$$3Eu(MQ)_3 + CaCO_3 \xrightarrow{TMB} [Eu_3(MQ)_7CO_3] + Ca(MQ)_2 \quad (3)$$

Thus, the elevated-temperature, pseudo-solid-state syntheses have potential to give mixed-ligand lanthanoid 8-quinaldinolates, in addition to their role in affording heterobimetallic complexes by Reactions (1) and (2).

Crystalline materials were identified mainly by X-ray crystallography (below) and powders by comparison of X-ray powder diffractograms with those generated from the single-crystal data. All infrared spectra were essentially the same, being totally dominated by the features of the MQ ligand, hence solvation by TMB or the presence of a single carbonate ligand had little effect. Contamination of single crystals by small amounts of powder made it difficult to obtain satisfactory samples for microanalysis. However, the near insolubility of the compounds in organic solvents enabled the powder to be washed away in representative cases, giving samples with satisfactory analytical data (Experimental Section).

Structural Studies

Trimetallic complexes $n[Ln_2Mg(MQ)_8]\cdot xTMB$ (Ln = Eu, Gd, Tb; n = 3, x = 1; Ln = Er; n = 1, x = 0) and $[Eu_2Mg(OQ)_8]$ crystallise in the triclinic space group $P\bar{1}$. For $3[Ln_2Mg(MQ)_8]\cdot TMB$ (Ln = Eu, Gd, Tb), one and a half trinuclear $[Ln_2Mg(MQ)_8]$ units and half a molecule of TMB are found in the asymmetric unit, and they are crystallographically unique. The three trimetallic units comprise one molecule Mg(1) (Scheme 1 and Figure S1) and two molecules Mg(2) (Figure 1) that are distinct from each other; only molecule Mg(1) possesses an inversion centre. $[Er_2Mg(MQ)_8]$ crystallises solely as a centrosymmetric molecule (Scheme 1 and Figure S2). Initially, this structure and those of the centrosymmetric molecule Mg(1) of $3[Ln_2Mg(MQ)_8]\cdot TMB$ are compared. In these, two octacoordinate lanthanoid atoms show a distorted dodecahedral (bisdisphenoidal) geometry. They are symmetry-related with the central alkaline earth metal positioned on a centre

of inversion. The Ln atoms have one terminal chelating (O, N) 8-quinaldinolate ligand and three chelating (O,N) 8-quinaldinolate ligands, which also bridge through their oxygen atoms to the central alkaline earth metal. The hexacoordinate alkaline earth metal is surrounded by the oxygen atoms in a distorted octahedral arrangement (Figure S1). This motif (Scheme 1) has previously been observed in $[Ln_2Ca(OQ)_8]$ (Ln = Nd, Eu) complexes,[12,14] and the connectivity is the same in molecule Mg(2) (Figure 1).

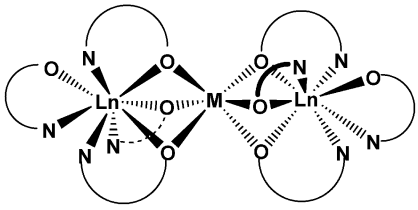

Scheme 1. Structural motif in trinuclear heterobimetallic 8-quinolinolate and 8-quinaldinolate complexes.

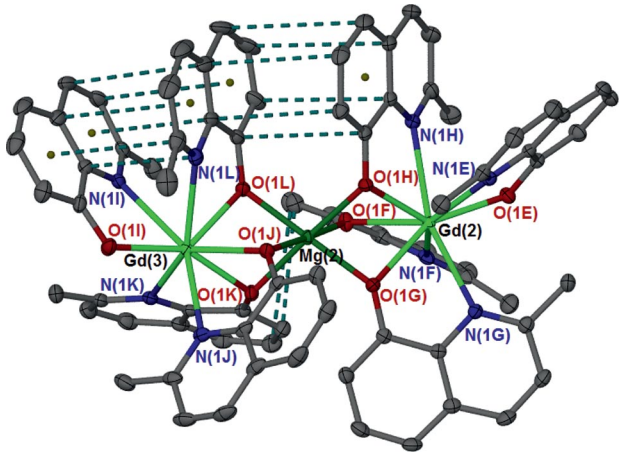

Figure 1. Molecular structure of molecule Mg(2) in $3[Gd_2Mg(MQ)_8]\cdot TMB$, representative also for Ln = Eu and Tb. Blue dashed lines indicate intramolecular offset and staggered π–π face-to-face interactions. Thermal ellipsoids are set at 50% probability. All hydrogen atoms are omitted for clarity.

Bond length data (Table 1) show a somewhat variable response to the decrease in ionic radii (0.062 Å)[16] from Eu^{3+} to Er^{3+}. Thus, for the average Ln–O_{br} (br = bridging) bond length, the decrease (2.35 → 2.29 Å) is as expected, whereas the contraction of the shorter Ln–O_{ter} (ter = terminal) bond lengths is smaller (2.27 → 2.24 Å). Three Ln–N bonds are associated with bridging ligands and one with a terminal ligand, the latter being marginally shorter than the average of the former. <Ln–N> bond lengths decrease by 0.078 Å over the series. As expected, the <Mg–O> bond lengths are not affected by changes in Ln (Table 1). More specifically, the individual Mg–O bond lengths are unsymmetrical in the solvated complexes but not in $[Er_2Mg(MQ)_8]$. The Mg–O bond lengths, 2.041(4)–2.121(5), exceed those [2.017(2)–2.063(2) Å (average)] of similarly bonded (μ-η^1:η^1) oxygen donor atoms of $[Mg_4(MQ)_4]$ (Figure 2, vide infra), which is possibly attributable to greater crowding in the heterobimetallics. The contraction of the nonbonding Ln···Mg···Ln distance over the series (Table 1) is approximately 0.2 Å, well above that expected from the lanthanoid contraction.

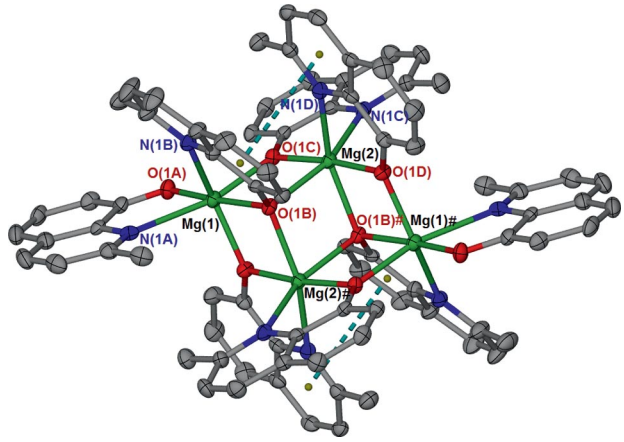

Figure 2. Crystal structure of $[Mg_4(MQ)_8]$. Dashed lines indicate intramolecular staggered π–π face-to-face interactions. Thermal ellipsoids are set at 50% probability. All hydrogen atoms are omitted for clarity. # indicates the symmetry operation $2 - x$, $1 - y$, $1 - z$.

In molecule Mg(1), three sets of intramolecular CH···π edge-to-face-like interactions can be found (Figure S1 and associated text). With the exclusion of the molecule of TMB of crystallisation in $[Er_2Mg(MQ)_8]$ (Figure S2), the ligands are involved in multiple intramolecular CH···π edge-to-face and π–π face-to-face interactions as well as an isolated case of intermolecular CH···π edge-to-face interaction (details in the Supporting Information).

Table 1. Selected bond lengths [Å] for molecule Mg(1) in $3[Ln_2Mg(MQ)_8]\cdot TMB$ (Ln = Eu, Gd, Tb) and for complex $[Er_2Mg(MQ)_8]$.

	$3[Eu_2Mg(MQ)_8]\cdot TMB$	$3[Gd_2Mg(MQ)_8]\cdot TMB$	$3[Tb_2Mg(MQ)_8]\cdot TMB$	$[Er_2Mg(MQ)_8]$
Ln(1)–O(1A)	2.271(4)	2.266(1)	2.257(5)	2.236(1)
Ln(1)–O(1B)	2.364(4)	2.347(2)	2.342(5)	2.283(1)
Ln(1)–O(1C)	2.345(4)	2.334(1)	2.324(5)	2.284(1)
Ln(1)–O(1D)	2.350(4)	2.339(2)	2.329(5)	2.318(1)
Ln(1)–N(1A)	2.623(5)	2.612(2)	2.601(7)	2.571(2)
Ln(1)–N(1B)	2.654(5)	2.628(2)	2.626(6)	2.546(1)
Ln(1)–N(1C)	2.718(5)	2.704(2)	2.698(6)	2.606(1)
Ln(1)–N(1D)	2.625(5)	2.603(2)	2.607(6)	2.595(2)
Mg(1)–O(1B)	2.041(4)	2.038(2)	2.041(5)	2.081(1)
Mg(1)–O(1C)	2.111(4)	2.105(1)	2.121(5)	2.096(1)
Mg(1)–O(1D)	2.107(4)	2.110(1)	2.119(5)	2.080(1)
Ln(1)–Mg(1)	3.194(1)	3.179(1)	3.174(1)	3.095(1)

Table 2. Selected bond lengths [Å] for molecule Mg(2) and complex $[Eu_2Mg(OQ)_8]$.

	$[Eu_2Mg(OQ)_8]$	$3[Eu_2Mg(MQ)_8]\cdot TMB$	$3[Gd_2Mg(MQ)_8]\cdot TMB$	$3[Tb_2Mg(MQ)_8]\cdot TMB$
Ln(2)–O(1E)	2.2925(13)	2.273(4)	2.2704(14)	2.252(5)
Ln(2)–O(1F)	2.3650(13)	2.357(4)	2.3465(15)	2.328(5)
Ln(2)–O(1G)	2.3829(13)	2.354(4)	2.3496(14)	2.333(5)
Ln(2)–O(1H)	2.3603(13)	2.341(4)	2.3275(14)	2.314(5)
Ln(2)–N(1E)	2.5729(16)	2.626(5)	2.6097(19)	2.606(7)
Ln(2)–N(1F)	2.5561(16)	2.668(5)	2.652(2)	2.640(6)
Ln(2)–N(1G)	2.5550(16)	2.668(5)	2.6574(17)	2.650(6)
Ln(2)–N(1H)	2.5767(16)	2.637(4)	2.6213(17)	2.617(7)
Mg(2)–O(1F)	2.0791(14)	2.048(4)	2.0511(16)	2.055(6)
Mg(2)–O(1G)	2.0550(14)	2.071(4)	2.0666(15)	2.069(6)
Mg(2)–O(1H)	2.1058(14)	2.094(4)	2.0936(15)	2.089(6)
Ln(2)–Mg(2)	3.2101(6)	3.196(2)	3.1826(10)	3.178(3)
Ln(3)–O(1I)	2.2999(13)	2.271(4)	2.2643(15)	2.237(5)
Ln(3)–O(1J)	2.3855(13)	2.356(4)	2.3374(15)	2.331(5)
Ln(3)–O(1K)	2.3481(13)	2.389(4)	2.3718(14)	2.359(5)
Ln(3)–O(1L)	2.3884(13)	2.336(4)	2.3154(14)	2.301(5)
Ln(3)–N(1I)	2.5427(16)	2.648(5)	2.6328(18)	2.622(6)
Ln(3)–N(1J)	2.5477(16)	2.650(4)	2.6398(17)	2.643(6)
Ln(3)–N(1K)	2.5902(15)	2.652(5)	2.639(2)	2.631(7)
Ln(3)–N(1L)	2.5414(16)	2.675(5)	2.6690(18)	2.668(7)
Mg(2)–O(1J)	2.0984(14)	2.060(4)	2.0809(16)	2.089(6)
Mg(2)–O(1K)	2.0617(14)	2.117(4)	2.1093(16)	2.110(6)
Mg(2)–O(1L)	2.0732(13)	2.088(4)	2.0797(15)	2.077(6)
Ln(3)–Mg(2)	3.2127(6)	3.170(2)	3.1549(9)	3.151(3)

For molecules Mg(2) (Figure 1), the coordination numbers and stereochemistry of the metal atoms are as in molecule Mg(1). The absence of an inversion centre in this trinuclear unit is reflected in the slightly bent Ln–Mg–Ln angle of 177.97(2)°. The asymmetry is also seen in unequal metal–metal distances [Ln(2)–Mg(2) is on average 0.027 Å longer than Ln(3)–Mg(2); Ln = Eu, Gd, Tb]. The related complex, $[Eu_2Mg(OQ)_8]$, also lacks a centre of symmetry and has an Eu–Mg–Eu angle of 176.34(2)°, but the metal–metal distances are effectively equal. From Ln = Eu to Ln = Tb, the decrease in Ln–O(N) bond lengths is similar to the decrease in ionic radius of 0.026 Å.[16] More interesting is a comparison with the bond lengths of the analogous $[Eu_2Mg(OQ)_8]$. The <Eu–N> distances of terminal and bridging ligands in $3[Eu_2Mg(MQ)_8]\cdot TMB$ are considerably longer than those in the OQ analogue. This increase is induced by the steric bulk of the methyl group in the 2-position. Concurrently, the rigidity of the ligand rotates the oxygen atom closer to the lanthanoid metal. Thus, <Eu–O> distances in $3[Eu_2Mg(MQ)_8]\cdot TMB$ are 0.02 Å shorter than the corresponding distances in the OQ complex. However, the central alkaline earth metal is not affected by the increased steric bulk, hence the more or less constant Mg–O distances in both the OQ and MQ derivatives. The Eu–Mg distances in the MQ structure are slightly shorter than those in the OQ analogue (Table 2), and this is probably related to the slight shortening of the bridging <Eu–O> distances.

A notable feature of the supramolecular interactions (Figure 1 and Supporting Information) is that π–π interactions are more extensive for ligands between Mg(2) and Gd(3) than between Mg(2) and Gd(2). This may account for the observation that the Ln(3)–Mg(2) distance is shorter (by ca. 0.03 Å) than the Ln(2)–Mg(2) distance.

Alternating layers of molecule Mg(1) and molecule Mg(2) can be observed along the crystallographic *c* axis; the layers propagate in the *ab* plane (Figure S3). The supramolecular interactions are considered in more detail in the Supporting Information.

Complex $[Mg_4(MQ)_8]$

This homometallic tetranuclear species comprises two crystallographically unique magnesium atoms that are each ligated in an octahedrally distorted manner by four oxygen and two nitrogen atoms from the 8-quinaldinolate ligands. There are two distinct coordination environments for each of the magnesium atoms. Mg(1) is surrounded by one terminal and two chelating-bridging ligands, whereas Mg(2) is exclusively coordinated by chelating-bridging ligands. As in the previous complexes, the bridging occurs solely through the oxygen atoms of the quinaldinolate ligands. A tridentate oxo-bridging mode [μ_3-η^2(N, O):η^1(O):η^1(O)] is observed for ligand B and for its symmetry-related equivalent B*. Ligands A and A* have a terminal role, whilst the remaining ligands have the more usual η^1(N)-μ-η^1:η^1(O) binding mode. The four magnesium atoms and the six oxygen atoms from the chelating-bridging ligands form a motif that is reminiscent of a cube.

Bond lengths (Table 3) of the terminal ligands Mg(1)–O(1A) and Mg(1)–N(1A) differ from the corresponding distances in the bridging-chelating ligands, being 0.10 Å shorter and 0.23 Å longer, respectively. The average Mg–O distance for the μ_3-η^1:η^1:η^1(O) ligand B is 2.17 Å and is approximately 0.13 Å longer than the corresponding distances for bidentate bridging Mg–O ligands C and D.

The sequence Mg–O(η^1) < Mg–O(η^1:η^1) < Mg–O(η^1:η^1:η^1) nicely reflects the involvement of one, two and three lone pairs, respectively.

Table 3. Selected bond lengths [Å] in $[Mg_4(MQ)_8]$.

	$[Mg_4(MQ)_8]$
Terminal	
M(1)–O(1A)	1.963(2)
M(1)–N(1A)	2.469(3)
Ligands with μ_3-η^1:η^1:η^1-O	
M(1)–O(1B)	2.149(2)
M(1)–N(1B)	2.281(3)
M(2)–O(1B)	2.205(2)
M(2)–O(1B)*	2.145(2)
Ligands with μ-η^1:η^1-O	
M(1)–O(1C)	2.063(2)
M(1)–O(1D)*	2.050(2)
M(2)–O(1C)	2.017(2)
M(2)–O(1D)	2.025(2)
M(2)–N(1C)	2.220(3)
M(2)–N(1D)	2.264(3)
Metal–metal	
M(1)–M(2)	3.240(2)
M(1)–M(2)*	3.265(1)
M(2)–M(2)*	3.282(2)

The supramolecular interactions (both intra and inter) are discussed in the Supporting Information. Remarkable is the close-to-parallel alignment of C(2A)/C(3A) with C(3D)*/C(2D)*, reflected in nearly equal distances of 3.58 and 3.51 Å. Each tetranuclear unit is connected to two adjacent tetranuclear units to form a 1D-chain type network through this interaction.

An isostructural Fe^{II} complex $[Fe_4(MQ)_8]$ has been synthesised by Sierau.[17]

Complexes $[Ln_2Ca(MQ)_8]$ (Ln = La, Eu)

The title complexes exhibit the same stoichiometry and similar structural features with the OQ analogues $[Ln_2Ca(OQ)_8]$ (Ln = Nd, Eu).[12,14] However, HMQ has succeeded where HOQ has so far failed in giving a lanthanum complex[18] (Figure 3).

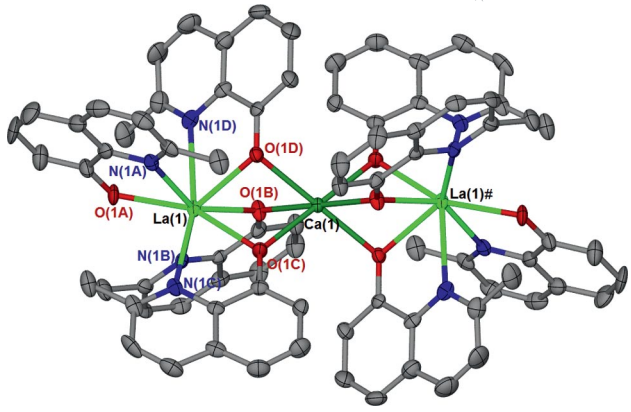

Figure 3. Crystal structure of $[La_2Ca(MQ)_8]$. All hydrogen atoms are omitted for clarity. Thermal ellipsoids are set at 50% probability. # indicates the symmetry operation $-x$, $1-y$, $1-z$.

Measured bond lengths are as expected (Table 4), and similar conclusions as for the $[Ln_2Mg(MQ)_8]$ series can be drawn. The MQ derivatives $[Ln_2Ca(MQ)_8]$ (Ln = La, Eu) exhibit increased <Ln–N> and shortened <Ln–O> and metal–metal distances relative to OQ complexes. For instance, in $[Eu_2Ca(OQ)_8]$, the average <Ln–N> distance for chelating-bridging ligands is shorter (by 0.10 Å) than that in $[Eu_2Ca(MQ)_8]$ (2.55 Å and 2.65 Å, respectively), whereas <Eu(1)–O(1)> for these ligands decreases by 0.04 Å from 2.39 Å to 2.35 Å, respectively. As mentioned above, this behaviour is attributed to the increased steric bulk from the methyl group in the 2-position. For $[La_2Ca(MQ)_8]$ and $[Eu_2Ca(MQ)_8]$, the contractions in terminal Ln(1)–O(1) and Ln(1)–N(1) distances (0.057 Å, 0.143 Å, respectively) lie on either side of ionic radii expectations (0.09 Å).[16] The influence of changing the alkaline earth metal is displayed in the increased average AE(1)–O(1) distance by 0.25 Å, 2.08 Å to 2.33 Å (Mg→Ca), in the Eu analogues $3[Eu_2Mg(MQ)_8]\cdot$TMB and $[Eu_2Ca(MQ)_8]$, respectively. The metal–metal distance is significantly influenced by the change in ligand. The Ln(1)–Ca(1) distance in $[Eu_2Ca(MQ)_8]$ is 0.07 Å shorter than that in $[Eu_2Ca(OQ)_8]$, 3.35 Å and 3.43 Å, respectively. Smaller but similar bond length changes were observed between isostructural Mg complexes $3[Eu_2Mg(MQ)_8]\cdot$TMB and $[Eu_2Mg(OQ)_8]$ (above). The

Table 4. Selected bond lengths [Å] in $[Ln_2Ca(MQ)_8]$ (Ln = La, Eu) and $[Ln_2Ca(OQ)_8]$ (Ln = Nd,[12] Eu[14]).

	$[La_2Ca(MQ)_8]$	$[Nd_2Ca(OQ)_8]$	$[Eu_2Ca(OQ)_8]$	$[Eu_2Ca(MQ)_8]$
Ln(1)–O(1A)	2.333(3)	2.335(4)	2.300(3)	2.276(5)
Ln(1)–O(1B)	2.472(3)	2.437(3)	2.402(3)	2.342(5)
Ln(1)–O(1C)	2.450(3)	2.431(3)	2.382(2)	2.351(5)
Ln(1)–O(1D)	2.443(3)	2.419(3)	2.386(3)	2.376(5)
Ln(1)–N(1A)	2.795(4)	2.602(4)	2.549(4)	2.652(6)
Ln(1)–N(1B)	2.847(3)	2.592(3)	2.556(3)	2.625(6)
Ln(1)–N(1C)	2.896(3)	2.610(4)	2.557(4)	2.675(6)
Ln(1)–N(1D)	2.765(3)	2.604(4)	2.564(4)	2.669(6)
Ca(1)–O(1B)	2.332(3)	2.321(3)	2.323(3)	2.336(5)
Ca(1)–O(1C)	2.347(3)	2.376(3)	2.303(3)	2.330(5)
Ca(1)–O(1D)	2.359(3)	2.309(3)	2.376(3)	2.334(5)
Ln(1)–AE(1)	3.5364(11)	3.4505(11)	3.433(1)	3.3563(13)

<Ca–O> distances are little affected by changing the ligand. However, since the oxygen–metal distances (Ln and AE) are now more asymmetric, the coordination geometry around the central alkaline earth metal atom results in an even more distorted octahedron than that for AE = Mg.

$[La_2Ca(MQ)_8]$ exhibits numerous CH···π edge-to-face and face-to-face π–π intermolecular interactions. The huge number and mode of connectivity of this network of interactions is likely to be responsible for the great stability of these type of complexes (M.p. >350 °C, air-stable). The details of these interactions are given in Figure S4 and the Supporting Information. Proceeding down in the series, $[Eu_2Ca(MQ)_8]$ displays significant changes in supramolecular interactions from the La derivative. Despite the unchanged stoichiometry, quite dramatic changes in the crystal packing and the appearance of the linear trinuclear unit occur. These are shown in Figures S5, S6 and considered in the accompanying discussion.

Complex $[Eu_3Ba(MQ)_{11}]$·2TMB

The tetranuclear $[Eu_3Ba(MQ)_{11}]$·2TMB is a new class of Ln/AE/MQ (or OQ) heterobimetallics and the first incorporating an alkaline earth metal heavier than calcium. Furthermore, the complex shows structural features different from those of the previous trinuclear homoleptic MQ/OQ complexes. A somewhat bent Eu(3)–Ba(1)–Eu(2) [159.202(6)°] array has a further europium atom Eu(1) bridging Ba(1) and Eu(2) (Figure 4) such that Eu(2) is displaced from linearity in response to the crowding caused by the Eu(1) bridge. The Ba(1)–Eu(1)–Eu(2) array is triangular with angles of 53.952(4)–63.391(4)°. All four metal atoms

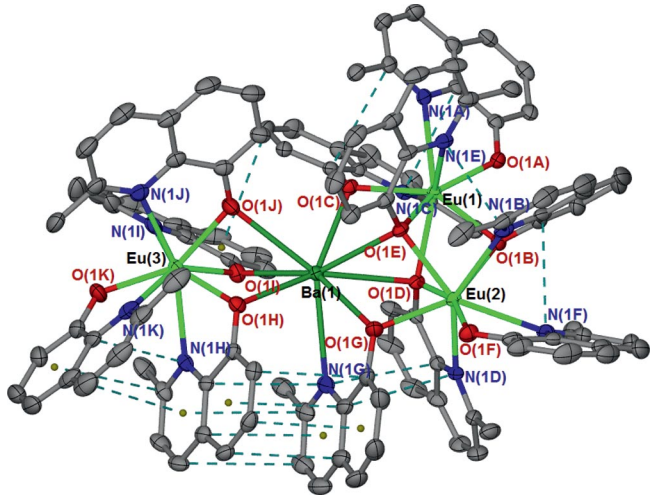

Figure 4. Asymmetric unit of $[Eu_3Ba(MQ)_{11}]$·2TMB. Blue dashed lines indicate intramolecular π–π face-to-face interactions. Thermal ellipsoids are set at 50% probability. All hydrogen atoms as well as the molecules of flux in the lattice are omitted for clarity.

Table 5. Selected bond lengths [Å] in $[Eu_3Ba(MQ)_{11}]$·2TMB.

	$[Eu_3Ba(MQ)_{11}]$·2TMB		
Terminal			
Eu(1)–O(1A)	2.258(2)	Eu(1)–N(1A)	2.715(3)
Eu(2)–O(1F)	2.256(2)	Eu(2)–N(1F)	2.695(3)
Eu(3)–O(1K)	2.290(2)	Eu (3)-N(1K)	2.654(3)
Bridging-chelating			
Eu(1)–O(1B)	2.377(2)		
Eu(1)–O(1C)	2.314(2)	Eu(1)–N(1C)	2.580(3)
Eu(2)–O(1B)	2.367(2)	Eu(2)–N(1B)	2.715(3)
Eu(3)–O(1H)	2.332(2)	Eu(3)–N(1H)	2.642(3)
Eu(3)–O(1I)	2.372(2)	Eu(3)–N(1I)	2.654(3)
Eu(3)–O(1J)	2.296(2)	Eu(3)–N(1J)	2.759(3)
Tridentate chelating-bridging			
Eu(1)–O(1D)	2.498(2)		
Eu(1)–O(1E)	2.435(2)	Eu(1)–N(1E)	2.643(3)
Eu(2)–O(1D)	2.465(2)	Eu(2)–N(1D)	2.622(2)
Eu(2)–O(1E)	2.386(2)		
Metal–metal			
Eu(1)–Ba(1)	3.9986(2)	Eu(3)–Ba(1)	3.8419(2)
Eu(2)–Ba(1)	4.0250(2)	Eu(1)–Eu(2)	3.6396(2)
Ba–O		Ba–Ligand	
Ba(1)–O(1C)	2.722(2)	Eu(2)–O(1G)	2.328(2)
Ba(1)–O(1D)	2.907(2)	Ba(1)–O(1G)	2.704(2)
Ba(1)–O(1E)	2.846(2)	Ba(1)–N(1G)	3.068(3)
Ba(1)–O(1H)	2.653(2)		
Ba(1)–O(1I)	2.716(2)		
Ba(1)–O(1J)	3.009(2)		

are octacoordinate, the behaviour of the large barium contrasting hexacoordination of Mg and Ca (Figure 1 and Figure 3). Both Eu(1) and Eu(2) possess one terminal MQ ligand, two chelating bidentate bridging ligands, as in 3[$Ln_2Mg(MQ)_8$]·TMB and [$Ln_2Ca(MQ)_8$], and two chelating and bridging tridentate [μ_3-η^2(N, O):η^1(O):η^1(O)] ligands, an arrangement hitherto not encountered in the homoleptic heterobimetallic Ln/AE/MQ (or OQ) complexes but observed for [$Mg_4(MQ)_8$] (Figure 2). Eu(3) has one terminal and three chelating-bridging ligands and is linked to Ba(1) as seen in the other structures (Scheme 1). Barium is coordinated by seven oxygen atoms, from five chelating-bridging ligands and two chelating-bridging tridentate ligands, and it is also ligated by a nitrogen atom from an MQ ligand that oxo-bridges between Ba(1) and Eu(2). Nitrogen bonding to the AE metal has not previously been observed in Ln/AE/MQ (above) (or OQ)[12,14] homoleptic complexes. Each of the two μ_3-η^2(N, O):η^1(O):η^1(O) MQ ligands bridges Ba(1), Eu(1), Eu(2) with one N-bonded to Eu(1) and one to Eu(2). One of the chelating-bridging ligands links Eu(1) and Eu(2) directly through oxygen with the nitrogen donor bound to Eu(2).

This tetranuclear unit and two molecules of 1,2,4,5-tetramethylbenzene are found in the asymmetric unit and are thus crystallographically unique. Moreover, one of the flux molecules is disordered over two positions over the inversion centre.

Because of the variety of binding modes exhibited by the MQ ligands, a wide variation of Eu/AE–O bond lengths is observed (Table 5). The average Eu–O bond length increase in the sequence terminal Eu–O (2.27 Å) < bridging Eu–O (2.34 Å) < bridging tridentate Eu–O (2.45 Å), corresponding to use of one, two, and three oxygen lone pairs, respectively. Although the associated average Eu–N bond lengths shows less variation (2.63–2.68 Å), the shortest are the Eu–N distances for the chelating-bridging tridentate ligands, compensating to a degree for the weaker Eu–O bonding. Surprisingly, the longest Ba–O bond length is not from an η^1:η^1:η^1-oxygen donor but from the η^1:η^1 bridging oxygen O(1J), possibly owing to steric repulsion between ligand J and the ligands bridging Ba(1) and Eu(1). Correspondingly, Eu(1)–O(1J) is the shortest Eu–O interaction with an η^1:η^1 bridging oxygen. The next two longest Ba–O distances involve η^1:η^1:η^1-oxygen donors. Unusually, O(1C) has a short bond to both Eu(1) and Ba(1).

Numerous intramolecular π–π face-to-face interactions can be found in this complex. The most developed one, a staggered π–π interaction, is observed between ligands H and G. The distances range from 3.55 to 3.22 Å. Numerous other π–π interactions of varying degree are found in this structure, and they are discussed in the Supporting Information.

Complexes [$Ln_3(MQ)_7CO_3$] (Ln = Eu, Er)

The serendipitous isolation of the carbonate moiety [$Er_3(MQ)_7CO_3$] (Figure 5) and the subsequent deliberate synthesis of its Eu analogue emphasise the versatility of the synthetic method.

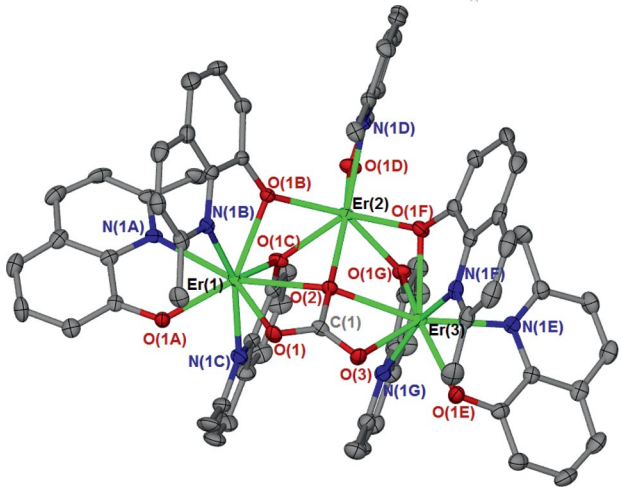

Figure 5. Asymmetric unit of [$Er_3(MQ)_7CO_3$]. Thermal ellipsoids are set at 50% probability. All hydrogen atoms are omitted for clarity.

In this trinuclear complex, the three lanthanoid atoms are gathered around a central CO_3 moiety, where peripheral Ln(1) and Ln(3) are octacoordinate, central Ln(2) is only heptacoordinate and Ln(1)–Ln(2) and Ln(2)–Ln(3) are approximately normal to each other in contrast to the linear trimetallics in Figures 1 and 3. Ln(1) and Ln(3) each are bound to one terminal (O, N) chelating 8-quinaldinolate ligand and two chelating-bridging (O, N) ligands; these ligands also bridge to the neighbouring Ln(2) metal. Ln(2) possesses one terminal chelating (O, N) ligand and four bridging oxygen atoms stemming from four adjacent chelating-bridging 8-quinaldinolate ligands. The central trigonal planar carbonate moiety is bound η^1(O)-μ_3:η^1:η^1:η^1(O′)-η^1(O″) to the three surrounding lanthanoid metals, completing their coordination spheres by chelating to each of the terminal Ln atoms and by unidentate binding to Ln(2). The coordination geometry around the octacoordinate atoms is a distorted dodecahedron (bisdisphenoid), and the heptacoordinate metal can be regarded as having distorted face-capped octahedral stereochemistry. There is considerable difference between this structure and those of [Ln_3(OQ or OQ′)$_8$(O_2CCH_3)] (Ln = Er, Yb; OQ′ = 5-chloro-8-quinolinolate),[7,15] in which an acetate ion chelates only to the central Ln atom. There are one terminal and three bridging-chelating OQ ligands on each outer Ln atom, and all Ln atoms are octacoordinate. The connectivity is reminiscent of [$Ln_3(OQ)_9$] complexes[9,10] an acetate replacing the terminal OQ of the central metal. The higher charge, smaller bulk and greater functionality of carbonate have led to a new structural class. With one less chelating-bridging MQ ligand between each pair of metals in [$Ln_3(MQ)_7CO_3$] than OQ ligands in [$Ln_3(OQ)_9$] (or [Ln_3(OQ or OQ′)$_8$-O_2CCH_3]), steric repulsion is much reduced, which enables closure of the Ln–Ln–Ln angle from linear to 90° to permit μ_3-carbonato coordination.

Bond lengths are given in Table 6. The contraction in <Ln–O> and <Ln–N> distances for terminal and chelating-bridging ligands (0.06–0.08 Å) from [$Eu_3(MQ)_7CO_3$] to

$[Er_3(MQ)_7CO_3]$ is close to the 0.06 Å lanthanoid contraction.[16] However, distances between metals [Ln(1)–Ln(2) and Ln(2)–Ln(3)] decrease by about 0.11 Å from an average of 3.57 Å in $[Eu_3(MQ)_7CO_3]$ to 3.46 Å in $[Er_3(MQ)_7CO_3]$, and the distance Ln(1)–Ln(3) reduces by 0.13 Å. The angle Ln(1)–Ln(2)–Ln(3) is 88.37° for Ln = Eu and 88.82° for Ln = Er. Terminal Ln–O and Ln–N bond lengths are shorter for Ln(2), which is attributable to the lower coordination number and less crowded situation. However, binding of bridging O donors shows no such differentiation. Both Ln–N and Ln–O bond lengths of the terminal Ln atoms are shorter than those in $3[Ln_2Mg(MQ)_8]\cdot TMB$ complexes (above). Although Ln is octacoordinate in each case, Ln(1) and Ln(3) are less crowded in the carbonate complex (Figure 5). Two different Ln–O bond lengths from the carbonate can be distinguished with Ln(1)–O(1) and Ln(3)–O(3) 0.09–0.17 Å shorter than Ln(1,2,3)–O(2). This is attributable to the $\eta^1{:}\eta^1{:}\eta^1$ behaviour of O(2), whereas O(1,3) each bind to a single Ln atom.

Table 6. Selected bond lengths [Å] for $[Ln_3(MQ)_7CO_3]$ (Ln = Eu, Er).

	$[Eu_3(MQ)_7CO_3]$	$[Er_3(MQ)_7CO_3]$
Terminal		
Ln(1)–O(1A)	2.2298(19)	2.173(2)
Ln(2)–O(1D)	2.2057(19)	2.155(2)
Ln(3)–O(1E)	2.232(2)	2.171(2)
Ln(1)–N(1A)	2.675(2)	2.604(3)
Ln(2)–N(1D)	2.573(2)	2.481(2)
Ln(3)–N(1E)	2.678(2)	2.602(3)
CO_3		
Ln(1)–O(1)	2.354(2)	2.294(2)
Ln(1)–O(2)	2.5354(19)	2.476(2)
Ln(2)–O(2)	2.4549(19)	2.3644(19)
Ln(3)–O(2)	2.5331(19)	2.461(2)
Ln(3)–O(3)	2.3704(19)	2.319(2)
Bridging		
Ln(1)–O(1B)	2.397(2)	2.325(2)
Ln(1)–O(1C)	2.3519(18)	2.290(2)
Ln(2)–O(1B)	2.3711(19)	2.308(2)
Ln(2)–O(1C)	2.3664(19)	2.297(2)
Ln(2)–O(1F)	2.397(2)	2.335(2)
Ln(2)–O(1G)	2.316(2)	2.247(2)
Ln(3)–O(1F)	2.417(2)	2.350(2)
Ln(3)–O(1G)	2.364(2)	2.306(2)
Ln(1)–N(1B)	2.638(2)	2.572(3)
Ln(1)–N(1C)	2.615(2)	2.542(3)
Ln(3)–N(1F)	2.641(2)	2.582(3)
Ln(3)–N(1G)	2.648(3)	2.590(3)
Metal–metal		
Ln(1)–Ln(2)	3.5859(2)	3.47476(19)
Ln(2)–Ln(3)	3.5653(2)	3.45898(19)
Ln(1)–Ln(3)	4.984	4.852

Conclusions

Rearrangement reactions of $Ln(MQ)_3$ and $AE(MQ)_2$ compounds at elevated temperatures in a TMB flux provide a useful route to homoleptic $[Ln_2AE(MQ)_8]$ complexes, and the new $[Eu_3Ba(MQ)_{11}]\cdot 2TMB$ has also been obtained by this method. The possibility of preparing mixed-ligand $[Ln_3(MQ)_7CO_3]$ complexes by analogous methods has been established and has potential for the inclusion of other small anions into $Ln(MQ \text{ or } OQ)_3$ complexes. Structural studies show chelating, chelating-bridging $\mu\text{-}\eta^2(N,O){:}\eta^1(O)$ and chelating tridentate $\mu\text{-}\eta^2(N,O){:}\eta^1(O){:}\eta^1(O)$ modes of binding for MQ ligands, whilst the carbonato complexes exhibit the very novel $\eta^1(O)\text{-}\mu_3\text{-}\eta^1(O'){:}(O'){:}(O')\text{-}\eta^1(O'')$ carbonate ligation. Typically, Ln atoms are octacoordinate, except for the heptacoordinate central metal of $[Ln_3(MQ)_7CO_3]$. Magnesium and calcium are hexacoordinate with solely O-atom binding, whilst barium is octacoordinate with seven oxygen and one nitrogen donor atoms in $[Eu_3Ba(MQ)_{11}]\cdot 2TMB$.

Experimental Section

Precursor metal 8-quinaldinolate complexes were prepared by mixing aqueous solutions of the metal chloride (either as purchased or from dissolution of the metal oxide in hydrochloric acid) and a stoichiometric amount of Na(MQ) (prepared by stoichiometric reaction of HMQ with NaOH in EtOH and subsequent concentration of the product), filtration and subsequent drying of the precipitated complex. ATR-IR spectra were obtained with a Specac ATR with a diamond anvil linked to a Bruker Equinox 55 a spectrometer fitted with a MCT detector. Powder XRD experiments (on mostly yellow to orange powders) were conducted using a Philips 1140 diffractometer with a Cu anode at λ = 1.5418 Å and a carbon monochromator. Powder samples were thoroughly ground in an agate mortar prior to measurement. Elemental analyses were performed by the Campbell Microanalytical Laboratories, University of Otago, New Zealand.

General Procedure: Syntheses of the complexes were achieved by heating the reaction mixture (ca. 0.50 g) with the desired stoichiometry of the precursor compounds and flux [1,2,4,5-tetramethylbenzene (TMB)] (1.0–1.7 g) in a sealed and evacuated thick-walled glass tube above 200 °C for several days. After visual examination confirmed that a reaction had occurred, the flux was removed from the reaction mixture by sublimation in an open-end oven at 150 °C for 2–4 h. The cooled tubes were opened in air and crystalline material (yellow crystals unless otherwise indicated) was handpicked from the bulk residual powder and characterised by single X-ray crystallography.

$[Mg_4(MQ)_8]$: A mixture of $La(MQ)_3$ (0.20 g, 0.30 mmol), $Mg(MQ)_2$ (0.05 g, 0.15 mmol) and TMB (1.00 g, 7.45 mmol) was heated to 210 °C and kept at that temperature for 21 d. Crystals of the title complex were handpicked from the bulk powder. Crystal yield: 0.007 g; 2.9%. M.p. >350 °C. IR: $\tilde{\nu}$ = 3047 (m), 1594 (w), 1558 (s), 1504 (s), 1462 (s), 1426 (vs), 1373 (s), 1325 (vs), 1307 (s), 1279 (s), 1099 (s), 831 (s), 735 (s) cm^{-1}. Powder XRD data on bulk powder (*d-spacing* [Å], rel. int.): *11.30* (46); *10.29* (100); *9.06* (25); *6.29* (46); *5.73* (32); *5.43* (25); *5.30* (22); *4.72* (24); *4.56* (43); *4.30* (22); *4.06* (26); *3.81* (27); *3.58* (23); *3.33* (43); *2.71* (26); *1.80* (58), closely resembled the generated powder pattern from single-crystal data.

$\{3[Eu_2Mg(MQ)_8](TMB)\}$

At 210 °C: A mixture of $Eu(MQ)_3$ (0.22 g, 0.30 mmol), $Mg(MQ)_2$ (0.05 g, 0.15 mmol) and TMB (1.00 g, 7.45 mmol) was heated to 210 °C and kept at that temperature for 21 d. Powder XRD mea-

surements showed formation of $[Mg_4(MQ)_8]$ as the major product as well as the unambiguous presence of the title complex. Powder XRD data on bulk powder (*d-spacing* [Å], rel. int.): *11.21* (38); *9.97* (100); *8.71* (33); *8.37* (42); *6.22* (42); *5.68* (21); *4.55* (24); *4.03* (34); *3.83* (36); *3.53* (27); *3.32* (31); *2.84* (17); *2.52* (18); *2.10* (17).

At 270 °C: A mixture of $Eu(MQ)_3$ (0.30 g, 0.47 mmol), $Mg(MQ)_2$ (0.08 g, 0.24 mmol) and TMB (1.50 g, 11.10 mmol) was initially heated to 270 °C and kept at that temperature for 18 d. The temperature was then decreased to 210 °C, kept there for 8 d, and finally it was lowered to 180 °C and kept there for 15 d. Large red crystals of the title complex were handpicked from the bulk powder. Crystal yield: 0.13 g; 32%. M.p. >350 °C. IR: $\tilde{\nu}$ = 3047 (m), 1592 (w), 1559 (s), 1503 (s), 1454 (vs), 1428 (vs), 1367 (s), 1326 (vs), 1300 (s), 1277 (vs), 1098 (s), 829 (s), 736 (s) cm^{-1}. $C_{250}H_{206}Eu_6Mg_3N_{24}O_{24}$ (4915.1): calcd. C 61.09, H 4.22, N 6.83; found C 61.12, H 4.31, N 6.76.

{3[$Gd_2Mg(MQ)_8$](TMB)}: A mixture of $Gd(MQ)_3$ (0.19 g, 0.30 mmol), $Mg(MQ)_2$ (0.05 g, 0.15 mmol) and TMB (1.00 g, 7.45 mmol) was heated to 210 °C and kept at that temperature for 21 d. Crystals of $[Mg_4(MQ)_8]$ (determined by unit cell comparison) alongside crystals of the title complex were handpicked from the bulk powder. Crystal yield: 0.04 g; 16%. M.p. >350 °C. IR: $\tilde{\nu}$ = 3046 (m), 1592 (w), 1559 (s), 1503 (s), 1452 (vs), 1428 (vs), 1367 (s), 1326 (vs), 1300 (s), 1277 (vs), 1098 (s), 829 (s), 737 (s) cm^{-1}. A sample of crystals for microanalysis corresponded to the title compound. $C_{250}H_{206}Gd_6Mg_3N_{24}O_{24}$ (4946.9): calcd. C 60.69, H 4.19, N 6.79; found C 61.38, H 4.34, N 6.99.

{3[$Tb_2Mg(MQ)_8$](TMB)}: A mixture of $Tb(MQ)_3$ (0.19 g, 0.30 mmol), $Mg(MQ)_2$ (0.05 g, 0.15 mmol) and TMB (1.00 g, 7.45 mmol) was heated to 210 °C and kept at that temperature for 21 d. Crystals of the title complex were handpicked from the bulk powder. Crystal yield: 0.05 g; 20%. M.p. >350 °C. IR: $\tilde{\nu}$ = 3046 (m), 1592 (w), 1560 (s), 1503 (s), 1456 (vs), 1429 (vs), 1368 (s), 1326 (vs), 1301 (s), 1278 (vs), 1099 (s), 830 (s), 737 (s) cm^{-1}. Powder XRD data on bulk powder showed that $[Mg_4(MQ)_8]$ formed only as minor product alongside the title complex. (*d-spacing* [Å], rel. int.): *11.18* (51); *10.51* (57); *9.60* (100); *8.49* (66); *8.11* (54); *7.19* (39); *6.29* (42); *5.45* (71); *5.10* (51); *4.43* (38); *4.29* (47); *4.01* (47); *3.85* (48); *3.79* (49); *3.16* (48); *3.47* (33); *2.02* (32); *1.65* (29). Some lines are possibly attributable to the presence of $[Mg_4(MQ)_8]$.

[$Er_2Mg(MQ)_8$]: $Er(MQ)_3$ (0.30 g, 0.46 mmol), $Mg(MQ)_2$ (0.08 g, 0.23 mmol) and TMB (1.70 g, 12.60 mmol) were initially heated to 270 °C and kept at that temperature for 18 d. The temperature was then decreased to 210 °C, kept there for 8 d, and finally it was lowered to 180 °C and kept at that temperature for 15 d. Crystals of $[Er_2Mg(MQ)_8]$ were handpicked from the bulk powder. Crystal yield: 0.03 g; 8%. M.p. >350 °C. IR: $\tilde{\nu}$ = 3035 (m), 1593 (w), 1559 (s), 1502 (s), 1459 (vs), 1424 (vs), 1372 (s), 1326 (s), 1302 (s), 1278 (s), 1099 (s), 830 (s), 737 (s) cm^{-1}. Powder XRD data on bulk powder (*d-spacing* [Å], rel. int.): *11.94* (23); *11.40* (49); *10.15* (100); *9.18* (29); *8.42* (15); *7.71* (37); *7.02* (22); *6.00* (17); *5.68* (18); *5.17* (21); *4.80* (26); *4.42* (39); *4.28* (32); *3.81* (19); *3.60* (54); *3.40* (18); *2.86* (20); *2.78* (18); *2.46* (13); *2.37* (14); *2.33* (14); *2.28* (13); *2.00* (12); *1.80* (12), indicating that the title complex had formed on a fairly large scale, phase-pure.

[$La_2Ca(MQ)_8$]: A mixture of $La(MQ)_3$ (0.30 g, 0.49 mmol), $Ca(MQ)_2$ (0.09 g, 0.25 mmol) and TMB (1.50 g, 11.17 mmol) was heated to 270 °C and kept at that temperature for 21 d. Crystals of the title complex were handpicked from the bulk powder. Crystal yield: 0.04 g; 11%. M.p. >350 °C. IR: $\tilde{\nu}$ = 3039 (m), 1591 (w), 1557 (s), 1502 (s), 1449 (vs), 1428 (vs), 1366 (s), 1327 (vs), 1299 (s), 1277 (vs), 1097 (s), 829 (s), 735 (s) cm^{-1}. $C_{80}H_{64}CaLa_2N_8O_8$ (1583.3): calcd. C 60.67, H 4.07, N 7.08; found C 60.86, H 4.11, N 7.12. Powder XRD data on bulk powder (*d-spacing* [Å], rel. int.): *11.33* (31); *9.38* (100); *8.68* (42); *4.82* (26); *4.39* (34); *4.28* (85); *3.87* (30); *3.56* (44); *3.24* (23); *3.13* (26); *2.76* (46); *2.14* (25), correspond well with values calculated from single-crystal data, showing only minor contamination by an unidentified crystalline material.

[$Eu_2Ca(MQ)_8$]: A mixture of $Eu(MQ)_3$ (0.19 g, 0.30 mmol), $Ca(MQ)_2$ (0.06 g, 0.15 mmol) and TMB (1.00 g, 7.45 mmol) was heated to 210 °C and kept at that temperature for 21 d. Crystals of the title complex were handpicked from the bulk powder. Crystal yield: 0.02 g, 16%. M.p. >350 °C. IR: $\tilde{\nu}$ = 3037 (m), 1591 (w), 1558 (s), 1502 (s), 1449 (vs), 1427 (vs), 1366 (s), 1328 (vs), 1299 (s), 1277 (vs), 1097 (s), 828 (s), 735 (s) cm^{-1}. The recorded powder XRD pattern indicated crystallinity, but no resemblance to the calculated powder pattern was detected.

[$Eu_3(MQ)_7(CO_3)$]: $Eu(MQ)_3$ (0.20 g, 0.32 mmol), $CaCO_3$ (0.05 g, 0.50 mmol) and TMB (1.00 g, 7.45 mmol) were sealed in an evacuated glass tube. The tube was initially heated to 120 °C and kept at that temperature for 7 d, then the temperature was increased to 200 °C and kept there for 24 d. Red crystals of $[Eu_3(MQ)_7(CO_3)]$ were handpicked from the bulk powder. Crystal yield: 0.04 g; 23%. M.p. >350 °C. IR: $\tilde{\nu}$ = 3040 (m), 1590 (w), 1557 (s), 1503 (s), 1455 (vs), 1430 (vs), 1369 (s), 1327 (vs), 1300 (s), 1277 (vs), 1099 (s), 831 (s), 734 (s) cm^{-1}.

[$Er_3(MQ)_7(CO_3)$]: $Er(MQ)_3$ (0.30 g, 0.46 mmol), $Ca(MQ)_2$ (0.08 g, 0.23 mmol) and TMB (1.50 g, 11.10 mmol) were initially heated to 270 °C and kept at that temperature for 18 d. The temperature was then decreased to 210 °C, kept there for 8 d, and finally it was lowered to 180 °C and kept at that temperature for 15 d. Red crystals of $[Er_3(MQ)_7(CO_3)]$ were handpicked from the bulk powder. Crystal yield: 0.06 g; 23%. M.p. >350 °C. IR: $\tilde{\nu}$ = 3039 (m), 1587 (w), 1557 (s), 1502 (s), 1456 (vs), 1427 (vs), 1370 (s), 1323 (vs), 1300 (s), 1270 (vs), 1099 (s), 828 (s), 739 (s) cm^{-1}. $C_{71}H_{56}Er_3N_7O_{10}$ (1669.0): calcd. C 51.09, H 3.38, N 5.87; found C 51.27, H 3.47, N 5.82. Powder XRD data on bulk powder (*d-spacing* [Å], rel. int.): *12.62* (100); *11.42* (79); *8.94* (67); *8.19* (32); *7.28* (32); *6.70* (28); *5.11* (31); *4.99* (34); *4.65* (26); *4.41* (49); *4.08* (31); *3.81* (38); *3.70* (32); *3.56* (32); *3.40* (35); *3.23* (31); *3.12* (30); *2.86* (32); *2.75* (32); *2.45* (29), corresponded with that calculated with some additional unidentified lines.

[$Eu_3Ba(MQ)_{11}$]·2TMB: A mixture of $Eu(MQ)_3$ (0.15 g, 0.23 mmol), $Ba(MQ)_2$ (0.05 g, 0.11 mmol) and TMB (1.00 g, 7.45 mmol) was heated to 210 °C and kept at that temperature for 7 d. Crystals of the title complex were handpicked from the bulk powder. Crystal yield: 0.015 g; 5%. M.p. >350 °C. Powder XRD data on bulk powder (*d-spacing* [Å], rel. int.): *18.64* (31); *15.61* (31); *14.62* (33); *14.02* (100); *12.44* (33); *11.84* (27); *11.13* (18); *10.65* (16); *10.18* (29); *9.88* (98); *8.68* (17); *8.18* (23); *7.75* (17); *6.88* (21); *6.28* (14); *5.56* (16); *5.44* (24); *4.78* (15); *4.13* (15); *3.90* (14); *3.61* (15); *3.46* (21); *3.35* (17); *3.13* (40); *2.91* (15); *2.71* (28), confirmed the presence of the title complex.

[$Eu_2Mg(OQ)_8$]: A mixture of $Eu(OQ)_3$ (0.15 g, 0.25 mmol), $Mg(OQ)_2$ (0.04 g, 0.13 mmol) and TMB (1.00 g, 7.45 mmol) were sealed in an evacuated glass tube. The tube was heated to 210 °C and kept at that temperature for 7 d. Crystals of the title complex were handpicked from the bulk powder. Crystal yield: 0.03 g; 15%. M.p. >350 °C. IR (Nujol mull): $\tilde{\nu}$ = 1722 (w), 1599 (m), 1568 (s), 1317 (m), 1280 (m), 1226 (w), 1169 (w), 1106 (s), 1029 (w), 962 (w), 862 (w), 823 (s), 804 (m), 786 (s), 644 (w) cm^{-1}. $C_{72}H_{48}Eu_2MgN_8O_8$ (1481.4): calcd. C 58.38, H 3.26, N 7.55; found C 58.45, H 3.28, N 7.51.

Direct Metal Reaction: Freshly filed La metal (0.30 g, 2.16 mmol), Mg metal turnings (0.10 g, 4.10 mmol), HMQ (0.75 g, 4.70 mmol) and elemental Hg (1 drop) were sealed in a tube with TMB (1.00 g, 7.45 mmol). The tube was heated up to 170 °C and left at that temperature for 21 d. No single crystals suitable for X-ray diffraction experiments could be retrieved. Powder XRD measurements were performed on the bulk residual powder and indicated that crystalline $[Mg_4(MQ)_8]$ was present, albeit on a small scale.

Crystallography

Low-temperature single-crystal X-ray diffraction experiments were performed with a Bruker Apex II KAPPA CCD or an Enraf Nonius Kappa CCD with Mo-K_α radiation (λ = 0.71073 Å) and equipped with an Oxford Instruments nitrogen gas cryostream. Single crystals were mounted on a glass fibre in viscous hydrocarbon oil. Crystals were quench-cooled to 123(2) K for all data sets except $[La_2Ca(MQ)_8]$, which was collected at 173 (1) K.

Analysis of diffraction data collected with the Bruker Apex II KAPPA CCD was performed by using SAINT+ within the APEX2[19] software package. Empirical absorption corrections were applied to all data by using SADABS.[20] Analysis of diffraction data collected with the Enraf Nonius Kappa CCD was performed by using DENZO.[21] Empirical absorption corrections were applied to all data using SORTAV[22] within WINGX.[23] The structures were solved using SHELXS[24] and refined using SHELXL-97[24] within the graphical interface X-SEED.[25] All non-hydrogen atoms in the structures were refined anisotropically, and hydrogen atoms were generated by using the riding model.

Special Refinement Details: For $[Eu_2Ca(MQ)_8]$, atom C1D was constrained by using the command ISOR 0.01; for $[Eu_3Ba(MQ)_{11}]\cdot 2TMB$, one molecule of TMB was disordered over two positions over the inversion centre and was freely refined by using the PART commands of SHELX (it was successfully refined to have approximate 60:40 occupancy).

CCDC-765408, -765409, -765410, -765411, -765412, -765413, -765414, -765415, -765416, -765417 and -765418 contain the supplementary crystallographic data for this paper. These data (excluding structure factors) can be obtained free of charge from The Cambridge Crystallographic Data Centre via www.ccdc.cam.ac.uk/data_request/cif.

A crystallographic table can be found at the end of the Supporting Information.

Crystal Data for $[Mg_4(MQ)_8]$: (CCDC-765415) $C_{80}H_{64}Mg_4N_8O_8$, M = 1362.63, yellow block, 0.15 × 0.10 × 0.10 mm^3, triclinic, space group $P\bar{1}$ (No. 2), a = 12.435(3) Å, b = 12.845(3) Å, c = 12.987(3) Å, α = 110.50(3)°, β = 117.03(3)°, γ = 94.57(3)°, V = 1658.3(11) Å^3, Z = 1, D_c = 1.364 g/cm^3, F(000) = 712, Nonius Kappa CCD, T = 123(1) K, $2\theta_{max}$ = 55.0°, 26279 reflections collected, 7614 unique (R_{int} = 0.0969). Final *GooF* = 0.967, *R1* = 0.0612, *wR2* = 0.1196, *R* indices based on 3658 reflections with $I > 2\sigma(I)$ (refinement on F^2), 455 parameters, 0 restraints. Lorentz polarization (LP) and absorption corrections applied, μ = 0.123 mm^{-1}.

Crystal Data for $3[Eu_2Mg(MQ)_8]\cdot TMB$: (CCDC-765412) $C_{250}H_{206}Eu_6Mg_3N_{24}O_{24}$, M = 4915.15, yellow block, 0.15 × 0.15 × 0.10 mm^3, triclinic, space group $P\bar{1}$ (No. 2), a = 13.046(3) Å, b = 16.237(3) Å, c = 26.824(5) Å, α = 100.66(3)°, β = 101.99(3)°, γ = 103.31(3)°, V = 5244(2) Å^3, Z = 1, D_c = 1.556 g/cm^3, F(000) = 2480, Nonius Kappa CCD, T = 123(1) K, $2\theta_{max}$ = 55.0°, 66712 reflections collected, 23826 unique (R_{int} = 0.0950). Final *GooF* = 0.998, *R1* = 0.0573, *wR2* = 0.1337, *R* indices based on 16447 reflections with $I > 2\sigma(I)$ (refinement on F^2), 1398 parameters, 0 restraints. LP and absorption corrections applied, μ = 1.852 mm^{-1}.

Crystal Data for $3[Gd_2Mg(MQ)_8]\cdot TMB$: (CCDC-765414) $C_{250}H_{206}Gd_6Mg_3N_{24}O_{24}$, M = 4946.86, yellow block, 0.25 × 0.25 × 0.07 mm^3, triclinic, space group $P\bar{1}$ (No. 2), a = 13.031(3) Å, b = 16.197(3) Å, c = 26.778(5) Å, α = 100.63(3)°, β = 101.97(3)°, γ = 103.35(3)°, V = 5217(2) Å^3, Z = 1, D_c = 1.574 g/cm^3, F(000) = 2486, Bruker X8 Apex II CCD, T = 123(1)K, $2\theta_{max}$ = 55.0°, 123221 reflections collected, 23606 unique (R_{int} = 0.0267). Final *GooF* = 1.036, *R1* = 0.0189, *wR2* = 0.0451, *R* indices based on 21758 reflections with $I > 2\sigma(I)$ (refinement on F^2), 1398 parameters, 0 restraints. LP and absorption corrections applied, μ = 1.966 mm^{-1}.

Crystal Data for $3[Tb_2Mg(MQ)_8]\cdot TMB$: (CCDC-765416) $C_{250}H_{206}Mg_3N_{24}O_{24}Tb_6$, M = 4956.84, yellow block, 0.20 × 0.20 × 0.15 mm^3, triclinic, space group $P\bar{1}$ (No. 2), a = 13.040(3) Å, b = 16.205(3) Å, c = 26.800(5) Å, α = 100.56(3)°, β = 102.03(3)°, γ = 103.40(3)°, V = 5226(2) Å^3, Z = 1, D_c = 1.575 g/cm^3, F(000) = 2492, Nonius Kappa CCD, T = 123(1)K, $2\theta_{max}$ = 55.0°, 76862 reflections collected, 23986 unique (R_{int} = 0.1591). Final *GooF* = 0.943, *R1* = 0.0633, *wR2* = 0.1054, *R* indices based on 11247 reflections with $I > 2\sigma(I)$ (refinement on F^2), 1398 parameters, 0 restraints. LP and absorption corrections applied, μ = 2.088 mm^{-1}.

Crystal Data for $[Er_2Mg(MQ)_8]$: (CCDC-765408) $C_{80}H_{64}Er_2MgN_8O_8$, M = 1624.22, yellow block, 0.15 × 0.15 × 0.13 mm^3, triclinic, space group $P\bar{1}$ (No. 2), a = 11.1075(2) Å, b = 12.3867(2) Å, c = 13.0308(3) Å, α = 75.8380(10)°, β = 73.8310(10)°, γ = 74.0250(10)°, V = 1627.79(5) Å^3, Z = 1, D_c = 1.657 g/cm^3, F(000) = 812, Bruker X8 Apex II CCD, T = 123(1) K, $2\theta_{max}$ = 55.0°, 28398 reflections collected, 7428 unique (R_{int} = 0.0222). Final *GooF* = 1.075, *R1* = 0.0157, *wR2* = 0.0393, *R* indices based on 7182 reflections with $I > 2\sigma(I)$ (refinement on F^2), 452 parameters, 0 restraints. LP and absorption corrections applied, μ = 2.638 mm^{-1}.

Crystal Data for $[La_2Ca(MQ)_8]$: (CCDC-765411) $C_{80}H_{64}CaLa_2N_8O_8$, M = 1583.29, yellow block, 0.20 × 0.15 × 0.15 mm^3, triclinic, space group $P\bar{1}$ (No. 2), a = 12.387(3) Å, b = 12.618(3) Å, c = 14.344(3) Å, α = 94.06(3)°, β = 115.24(3)°, γ = 114.04(3)°, V = 1769.1(12) Å^3, Z = 1, D_c = 1.486 g/cm^3, F(000) = 798, Nonius Kappa CCD, T = 173(1)K, $2\theta_{max}$ = 55.0°, 23579 reflections collected, 7984 unique (R_{int} = 0.0601). Final *GooF* = 0.899, *R1* = 0.0448, *wR2* = 0.1026, *R* indices based on 6177 reflections with $I > 2\sigma(I)$ (refinement on F^2), 452 parameters, 0 restraints. LP and absorption corrections applied, μ = 1.326 mm^{-1}.

Crystal Data for $[Eu_2Ca(MQ)_8]$: (CCDC-765413) $C_{80}H_{64}CaEu_2N_8O_8$, M = 1609.39, yellow block, 0.15 × 0.15 × 0.10 mm^3, triclinic, space group $P\bar{1}$ (No. 2), a = 11.101(2) Å, b = 12.546(3) Å, c = 13.348(3) Å, α = 76.66(3)°, β = 73.97(3)°, γ = 73.41(3)°, V = 1688.9(6) Å^3, Z = 1, D_c = 1.582 g/cm^3, F(000) = 810, Nonius Kappa CCD, T = 123(1)K, $2\theta_{max}$ = 55.0°, 25958 reflections collected, 7773 unique (R_{int} = 0.1862). Final *GooF* = 0.979, *R1* = 0.0733, *wR2* = 0.1019, *R* indices based on 3713 reflections with $I > 2\sigma(I)$ (refinement on F^2), 452 parameters, 12 restraints. LP and absorption corrections applied, μ = 1.982 mm^{-1}.

Crystal Data for $[Er_3(MQ)_7CO_3]$: (CCDC-765409) $C_{71}H_{56}Er_3N_7O_{10}$, M = 1669.01, red block, 0.25 × 0.20 × 0.20 mm^3, monoclinic, space group $P2_1/c$ (No. 14), a = 13.5552(2) Å, b = 23.4514(3) Å, c = 19.6923(2) Å, β = 106.3520(10)°, V =

6006.74(13) Å^3, Z = 4, D_c = 1.846 g/cm^3, F(000) = 3260, Bruker X8 Apex II CCD, T = 123(1) K, $2\theta_{max}$ = 55.0°, 68189 reflections collected, 13801 unique (R_{int} = 0.0426). Final *GooF* = 1.017, *R1* = 0.0239, *wR2* = 0.0466, *R* indices based on 11514 reflections with $I > 2\sigma(I)$ (refinement on F^2), 827 parameters, 0 restraints. LP and absorption corrections applied, μ = 4.223 mm^{-1}.

Crystal Data for [Eu$_3$(MQ)$_7$CO$_3$]: (CCDC-765410) $C_{71}H_{56}Eu_3N_7O_{10}$, M = 1623.11, red block, 0.15 × 0.15 × 0.10 mm^3, monoclinic, space group $P2_1/c$ (No. 14), a = 13.6229(3) Å, b = 23.7329(5) Å, c = 19.6912(4) Å, β = 106.2920(10)°, V = 6110.7(2) Å^3, Z = 4, D_c = 1.764 g/cm^3, F(000) = 3200, Bruker X8 Apex II CCD, T = 123(1) K, $2\theta_{max}$ = 55.0°, 85926 reflections collected, 14015 unique (R_{int} = 0.0516). Final *GooF* = 1.011, *R1* = 0.0252, *wR2* = 0.0459, *R* indices based on 11264 reflections with $I > 2\sigma(I)$ (refinement on F^2), 827 parameters, 0 restraints. LP and absorption corrections applied, μ = 3.110 mm^{-1}.

Crystal Data for [Eu$_3$Ba(MQ)$_{11}$]·2TMB: (CCDC-765417) $C_{130}H_{116}BaEu_3N_{11}O_{11}$, M = 2601.56, yellow block, 0.13 × 0.10 × 0.10 mm^3, monoclinic, space group $P2_1/c$ (No. 14), a = 18.5213(4) Å, b = 21.1756(5) Å, c = 28.5103(8) Å, β = 93.6090(10)°, V = 11159.6(5) Å^3, Z = 4, D_c = 1.548 g/cm^3, F(000) = 5224, Bruker X8 Apex II CCD, T = 123(1) K, $2\theta_{max}$ = 55.0°, 92143 reflections collected, 25496 unique (R_{int} = 0.0379). Final *GooF* = 1.036, *R1* = 0.0314, *wR2* = 0.0665, *R* indices based on 21176 reflections with $I > 2\sigma(I)$ (refinement on F^2), 1519 parameters, 1 restraint. LP and absorption corrections applied, μ = 2.079 mm^{-1}.

Crystal Data for [Eu$_2$Mg(OQ)$_8$]: (CCDC-765418) $C_{72}H_{48}Eu_2MgN_8O_8$, M = 1481.41, yellow prism, 0.30 × 0.13 × 0.13 mm^3, triclinic, space group $P\bar{1}$ (No. 2), a = 12.4728(2) Å, b = 13.6512(2) Å, c = 18.4438(3) Å, α = 94.7910(10)°, β = 95.6600(10)°, γ = 100.5240(10)°, V = 3055.93(8) Å^3, Z = 2, D_c = 1.610 g/cm^3, F(000) = 1476, Bruker X8 Apex II CCD, T = 123(1) K, $2\theta_{max}$ = 55.0°, 54708 reflections collected, 14009 unique (R_{int} = 0.0239). Final *GooF* = 1.060, *R1* = 0.0190, *wR2* = 0.0452, *R* indices based on 12423 reflections with $I > 2\sigma(I)$ (refinement on F^2), 820 parameters, 0 restraints. LP and absorption corrections applied, μ = 2.110 mm^{-1}.

Supporting Information (see footnote on the first page of this article): A detailed description of intra- and intermolecular π–π interactions, crystal packing as well as a crystallographic table of the complexes.

Acknowledgments

We are grateful to the Australian Research Council for funding this research (ARC DP DP0984775).

[1] R. G. W. Hollingshead, *Oxine and Its Derivatives, Vol. 1*, Butterworths, London, **1954**.
[2] M. Albrecht, Y. Liu, S. S. Zhu, C. A. Schalley, R. Froehlich, *Chem. Commun.* **2009**, 1195–1197.
[3] J.-C. G. Bünzli, C. Piguet, *Chem. Soc. Rev.* **2005**, *34*, 1048–1077.
[4] N. M. Shavaleev, R. Scopelliti, F. Gumy, J.-C. G. Bünzli, *Inorg. Chem.* **2009**, *48*, 2908–2918.
[5] M. Giraud, E. S. Andreiadis, A. S. Fisyuk, R. Demadrille, J. Pecaut, D. Imbert, M. Mazzanti, *Inorg. Chem.* **2008**, *47*, 3952–3954.
[6] M. A. Katkova, Y. A. Kurskii, G. K. Fukin, A. S. Averyushkin, A. N. Artamonov, A. G. Vitukhnovsky, M. N. Bochkarev, *Inorg. Chim. Acta* **2005**, *358*, 3625–3632.
[7] R. Van Deun, P. Fias, P. Nockemann, A. Schepers, T. N. Parac-Vogt, K. Van Hecke, L. Van Meervelt, K. Binnemans, *Inorg. Chem.* **2004**, *43*, 8461–8469.
[8] M. A. Katkova, V. A. Ilichev, A. N. Konev, M. N. Bochkarev, A. G. Vitukhnovsky, M. A. Parshin, L. Pandey, M. Van der Auweraer, *J. Appl. Phys.* **2008**, *104*, 053706, 3pp..
[9] F. Artizzu, P. Deplano, L. Marchio, M. L. Mercuri, L. Pilia, A. Serpe, F. Quochi, R. Orru, F. Cordella, F. Meinardi, R. Tubino, A. Mura, G. Bongiovanni, *Inorg. Chem.* **2005**, *44*, 840–842.
[10] S. G. Leary, G. B. Deacon, P. C. Junk, *Z. Anorg. Allg. Chem.* **2005**, *631*, 2647–2650.
[11] M. A. Katkova, V. A. Ilichev, G. K. Fukin, M. N. Bochkarev, *Inorg. Chim. Acta* **2009**, *362*, 1393–1395.
[12] G. B. Deacon, P. C. Junk, S. G. Leary, *Z. Anorg. Allg. Chem.* **2004**, *630*, 1541–1543.
[13] G. B. Deacon, C. M. Forsyth, P. C. Junk, S. G. Leary, *New J. Chem.* **2006**, *30*, 592–596.
[14] G. B. Deacon, C. M. Forsyth, P. C. Junk, U. Kynast, G. Meyer, J. Moore, J. Sierau, A. Urbatsch, *J. Alloys Compd.* **2008**, *451*, 436–439.
[15] E. Silina, Y. Bankovsky, V. Belsky, J. Lejejs, L. Peck, *Latv. Khim. Zh.* **1997**, 89.
[16] R. D. Shannon, *Acta Crystallogr., Sect. A* **1976**, *32*, 751–767.
[17] J. Sierau, Dissertation Thesis, University of Cologne, **2008**.
[18] S. G. Leary, Ph. D. Thesis, Monash University, **2005**.
[19] *APEX II Program Suite*, Bruker AXS Ltd., Madison, WI, **2005**.
[20] G. M. Sheldrick, *SADABS, Empirical Absorption Corrections Program for Area Detector Data*, University of Göttingen, Germany, **1996**.
[21] Z. Otwinowski, W. Minor, *Methods Enzymol.* **1997**, *276*, 307.
[22] R. H. Blessing, *Acta Crystallogr., Sect. A* **1995**, *51*, 33.
[23] L. J. Farrugia, *J. Appl. Crystallogr.* **1999**, *32*, 837.
[24] G. M. Sheldrick, *SHELXS-97 and SHELXL-97*, University of Göttingen, Germany, **1997**.
[25] L. J. Barbour, *J. Supramol. Chem.* **2001**, *1*, 189.

Received: March 24, 2010
Published Online: May 26, 2010

